Human Gut Microbial Sulfonolipids are linked to Inflammatory Bowel Diseases through Toll-Like Receptor 4 Signaling

Ethan A. Older[1,7], Jian Zhang[2,3,7], Zachary E. Ferris[1], Dan Xue[1], Zheng Zhong[2,3], Mary K. Mitchell[4], Michael Madden[1], Yuzhen Wang[5], Hexin Chen[4], Prakash Nagarkatti[6], Mitzi Nagarkatti[6], Daping Fan[5], Melissa Ellermann[4], Yong-Xin Li[2,3]* and Jie Li[1]*

[1]Department of Chemistry and Biochemistry, University of South Carolina, Columbia, South Carolina, USA. [2]Department of Chemistry and The Swire Institute of Marine Science, The University of Hong Kong, Pokfulam Road, Hong Kong, China. [3]Southern Marine Science and Engineering Guangdong Laboratory (Guangzhou), Guangzhou, China. [4]Department of Biological Sciences, University of South Carolina, Columbia, South Carolina 29209, United States. [5]Department of Cell Biology and Anatomy, School of Medicine, University of South Carolina, Columbia, South Carolina 29209, United States. [6]Department of Pathology, Microbiology and Immunology, School of Medicine, University of South Carolina, Columbia, South Carolina 29209, United States

[7]These authors contributed equally to this work.

*To whom correspondence may be addressed.

Email: yxpli@hku.hk; li439@mailbox.sc.edu

Abstract

The trillions of microorganisms inhabiting the human gut are intricately linked to human health. At the species abundance level, correlational studies have connected specific bacterial taxa to various diseases. While the abundances of these bacteria in the gut serve as good indicators for disease progression, understanding the functional metabolites they produce is critical to decipher how these microbes influence human health. Here, we leverage multi-omics big data analysis to directly establish a negative correlation between sulfonolipid (SoL) biosynthesis in the human gut microbiome and inflammatory bowel disease (IBD). We experimentally validate this informatic correlation in a mouse model of IBD, showing that SoLs are produced in higher abundance in non-IBD mice compared to IBD mice. We determine that SoLs consistently contribute to the immunoregulatory activity of SoL-producing human gut commensal strains. We further reveal that sulfobacin A (SoL A), a representative member of SoLs, primarily mediates its dual immunomodulatory activity through Toll-like receptor 4 (TLR4). We also demonstrate that SoL A interacts with TLR4 via direct binding to myeloid differentiation factor 2 and that SoL A competes with the natural ligand, lipopolysaccharide, for binding. Together, these results suggest that SoLs mediate a protective effect against IBD through TLR4 signaling and also showcase a widely applicable informatics-based approach to directly linking the biosynthesis of functional metabolites to human health.

Introduction

The human gut microbiome, composed of trillions of microorganisms, is increasingly recognized as having a significant influence on human health through the production of numerous functional metabolites that are in direct contact and constant exchange with host cells[1]. The metabolism at the human-microbiota interface is formed and regulated by the long-term symbiosis and co-evolution between humans and microbes, thus inherently linking human microbial functional metabolites to human health[2–5]. A remarkable class of such metabolites is microbe-derived lipids. Biosynthesized *de novo* by human gut microbiota or biotransformed from dietary nutrients, these lipids can be directly sensed by the host to modulate both metabolic and immunological pathways[6].

In our search for underexplored functional lipid metabolites produced at the human-microbiota interface, our attention was drawn to *Alistipes* and *Odoribacter*, two commensal genera of the human gut microbiome with emerging significance in modulating health, particularly in the two primary forms of inflammatory bowel diseases (IBD): ulcerative colitis (UC) and Crohn's disease (CD)[7–10]. Species abundances of members of both genera have been found to negatively correlate with IBD pathogenesis, suggesting that they may play a protective role against IBD[7,8]. Additionally, some species have been shown to ameliorate symptoms of IBD[9,10]. Notably, both *Alistipes* and *Odoribacter* are prolific sulfonolipid (SoL) producers[11]. SoLs are unique lipid molecules that bear striking structural similarity to both bacterial and endogenous sphingolipids (SLs), which are known for their role in mediating immune signaling in the human body[12]. Species from *Alistipes* and *Odoribacter* do not produce SLs[11,13]. Instead, SoLs are produced in high abundance in these species[11,14].

The replacement of SLs by structurally related SoLs in *Alistipes* and *Odoribacter* suggests that SoLs may serve as functional metabolites and exert similar but distinctly different functions compared to their SL cousins. In fact, we have found that sulfobacin A (SoL A) produced by *Chryseobacterium gleum* F93 DSM 16776, a representative of human microbial SoLs, exhibits unusual dual immunomodulatory activity *in vitro* by modulating inflammatory cytokine production, especially through suppression of the lipopolysaccharide (LPS)-induced inflammatory response[15]. However, the mechanism of SoLs' anti-inflammatory effect against LPS is unknown. Importantly, LPS is a notorious inducer of strong pro-inflammatory responses via activation of the Toll-like

receptor 4 (TLR4) pathway and LPS-TLR4 signaling activation has been reported as a key contributor to the progression of IBD[16–19]. Whether SoLs produced by *Alistipes* and *Odoribacter*, two genera known to be negatively associated with IBD, play a role in this negative correlation through suppression of LPS signaling is also unknown.

Thus, we set out to investigate the association between SoLs biosynthesis and IBD pathogenesis as well as the mechanism of action of SoLs as a potential explanation for the protective effects of *Alistipes* and *Odoribacter* against IBD. Since the functional metabolites are encoded by biosynthetic genes, we leveraged publicly available metagenomic and metatranscriptomic big data of biosynthetic genes, combined with metabolomics, to reveal a negative correlation directly between SoLs biosynthesis and human IBD pathogenesis. We experimentally validated this informatic correlation using a mouse model of IBD. Through bioactivity-guided fractionation and scoring, we determined that SoLs consistently contribute to the immunoregulatory activity of SoL-producing human gut commensals. Using cell-based assays, we also revealed that SoL A primarily mediates its dual immunomodulatory activity through interaction with TLR4. We further demonstrated that SoL A binds directly to TLR4 via the accessory protein myeloid differentiation factor 2 (MD-2) and displaces LPS from MD-2 at higher concentrations. Together, our results demonstrate an informatics-based, functional metabolites-focused approach to uncovering the chemical basis and molecular mechanisms of intricate host-microbe interactions and outline a potential mechanism by which *Alistipes* and *Odoribacter*-derived SoLs exert a protective effect against IBD progression through disruption of LPS-TLR4 signaling.

Results

Multi-omics analysis reveals a negative correlation between SoLs biosynthesis and IBD. We began by systematically investigating the biosynthetic potential of SoLs from 285,835 human gut bacterial reference genomes including single amplified genomes (SAGs) and metagenome-assembled genomes (MAGs)[20]. Based on sequence homology with experimentally verified SoL biosynthetic enzymes[15,21–23], we identified a total of 562,214 homologous enzyme sequences, including 469,012 cysteate synthases (CYS), 33,486 cysteate fatty acyltransferases (CFAT), and 59,716 short-chain dehydrogenases/reductases (SDR) (**Supplementary Fig. 1a**).

Uncovering phylogenetic trends, we found that these three enzymes were widely distributed in 255,572 genomes across 21 phyla, with the majority belonging to Bacteroidota and Firmicutes A (**Supplementary Fig. 1b**). A subset of 6.21% (15,863/255,572) of the genomes was found to encode all three putative SoL biosynthetic enzymes (**Supplementary Fig. 1a**). To prioritize them for further analysis, we filtered the homologs on the basis of three rules: (1) the homology of both CFAT and CYS must equal or exceed 50% sequence similarity with experimentally validated CFATs and CYSs (**Supplementary Table 1**), as these enzymes are the first two specific enzymes in the biosynthetic pathway of SoLs that distinguish the biosynthesis between SoLs and SLs[15,21–23]; (2) the homologous regions of CYS, CFAT, and SDR should include protein domains with Pfam IDs PF00291, PF00155, and PF00106, respectively (hit score > 50); (3) a set of homologous enzymes, especially SDR enzymes that show variable sequence similarities, should come from the same genome encoding all three enzymes as all three are required for SoL biosynthesis, thus ensuring co-occurrence. Applying these rules, we prioritized 9,731 CYS (1,384 unique sequences), 9,740 CFAT (917 unique sequences), and 10,319 SDR enzymes (1,076 unique sequences) (**Fig. 1a**, **Supplementary Data 1**) from 9,633 bacterial genomes. The prioritized enzymes were distributed among 43 species from Bacteroidota and one species from Firmicutes A (**Fig. 1b**, **Supplementary Data 2**). Of note, among the 42 species from Bacteroidota, 71% (30/42) of them belonged to bacterial families that have been previously reported to produce SoLs (**Fig. 1b**) including *Rikenellaceae* (containing genera *Alistipes* and *Alistipes*_A)[11,24], *Marinifilaceae* (containing genus *Odoribacter*)[11], and *Weeksellaceae* (containing genus *Chryseobacterium* B)[15,25].

To determine whether there is a link between the capacity of the human gut microbiome to produce SoLs and IBD, we conducted a comparative analysis of metagenomic and metatranscriptomic data obtained from the Inflammatory Bowel Disease Multi'omics Database (IBDMDB, https://ibdmdb.org/)[8,26]. We began by generating sequence similarity networks with a 90% sequence identity threshold to group enzymes with similar functions. Consequently, we categorized the prioritized biosynthetic enzymes into 214 subfamilies (79 CYS subfamilies; 25 CFAT subfamilies; 110 SDR subfamilies) for the subsequent analyses (**Supplementary Table 2**). Looking for the presence of the prioritized 214 subfamilies in IBD cohorts, we identified 154 subfamilies in 667 metagenome samples (182 healthy samples and 485 IBD disease samples), of which 116 subfamilies were detected in more

than ≥ 5% of samples (**Supplementary Fig. 1c**). Beta diversity of the presence of these 116 subfamily biosynthetic enzymes indicated that the overall composition of SoL biosynthetic enzyme subfamilies was significantly different between the healthy and IBD cohorts (**Fig. 1c**, Jaccard distance, PERMANOVA $p = 0.001$). Of note, 57 subfamilies had a significantly higher prevalence (Fisher's exact test $p < 0.05$) in healthy individuals as compared to IBD cases (**Supplementary Table 3**), among which 35 subfamilies (18 CYS subfamilies, 2 CFAT subfamilies, and 15 SDR subfamilies) further show a difference of prevalence > 10% (**Fig. 1d**).

To further examine the difference between the expression profiles of SoL biosynthetic enzymes between the IBD and healthy groups, we extended our comparative analysis to the metatranscriptomic level. We found that 132 SoL biosynthetic enzyme subfamilies were expressed in 777 metatranscriptomic samples (193 healthy samples, 584 IBD disease samples), with about 42% (55/132) detected in at least 5% of samples (**Supplementary Fig. 1d**). Beta diversity of the expression profiles of SoL biosynthetic enzymes suggested that the overall expression of these enzyme subfamilies is significantly different between the healthy and IBD cohorts (**Fig. 1c**, Bray-Curtis distance, PERMANOVA $p = 0.001$). To capture more detail, we compared the prevalence and abundance differences of each enzyme subfamily in the metatranscriptomic samples. Nine subfamilies had higher prevalence (Fisher's exact test $p < 0.05$, varying from 9% ~ 17%) in the non-IBD group than the IBD group (**Supplementary Table 4**). We further identified 8 subfamilies (6 CYS, 1 CFAT, and 1 SDR) as significantly different in abundance (expression) profiles between the healthy controls and IBD cases (**Fig. 1f**, two-sided Mann-Whitney *U* test, adjusted $p < 0.05$). Notably, 7 of the 8 subfamilies had a higher prevalence (**Fig. 1f,** upper panel, Fisher's exact test $p < 0.05$) and a higher abundance (**Fig. 1f**, lower panel, one-sided Mann-Whitney *U* test, adjusted $p < 0.05$) in the non-IBD group than in the IBD group.

We finally looked for metabolomic evidence in the differences of detectable SoLs, the products of the biosynthetic enzymes mentioned above, among IBD and non-IBD groups from publicly accessible metabolomics datasets. We expected that the increased expression of SoL biosynthetic enzymes would correspond with increased production of SoLs in non-IBD groups compared to IBD groups. Using metabolomics data from IBDMDB first, three metabolite features were assigned to Sulfobacins B (SoL B), C (SoL C), and F (SoL F) by exact mass comparison with mass error less than 5ppm (**Supplementary Data 3**). Indeed, we found that SoLs B,

C, and F had significantly higher abundance in non-IBD groups than IBD groups (**Fig. 1g**, Wilcoxon rank sum test, $p < 0.001$). Furthermore, higher SoLs B, C, and F abundance in non-IBD samples was observed compared to both IBD subtypes: Ulcerative colitis (UC) and Crohn's disease (CD) (**Supplementary Fig. 2**, Wilcoxon rank sum test , $p < 0.001$). In another independent metabolomics dataset[27], we found that the abundance of SoL B was also lower in IBD groups, consistent with the result generated from the first dataset (**Supplementary Fig. 3**, Wilcoxon rank sum test, $p < 0.001$).

Thus, our metagenomic analysis reflects that SoL biosynthetic enzymes are more prevalent in non-IBD groups than IBD groups, metatranscriptomics suggests that these enzymes are more actively transcribed in non-IBD groups, and metabolomics indicates that representative SoLs are produced in higher abundance in non-IBD groups. Altogether, our findings establish a negative correlation directly between SoLs biosynthesis and IBD, consistent with previously reported negative association between SoL-producers, namely *Alistipes* and *Odoribacter*, and IBD.

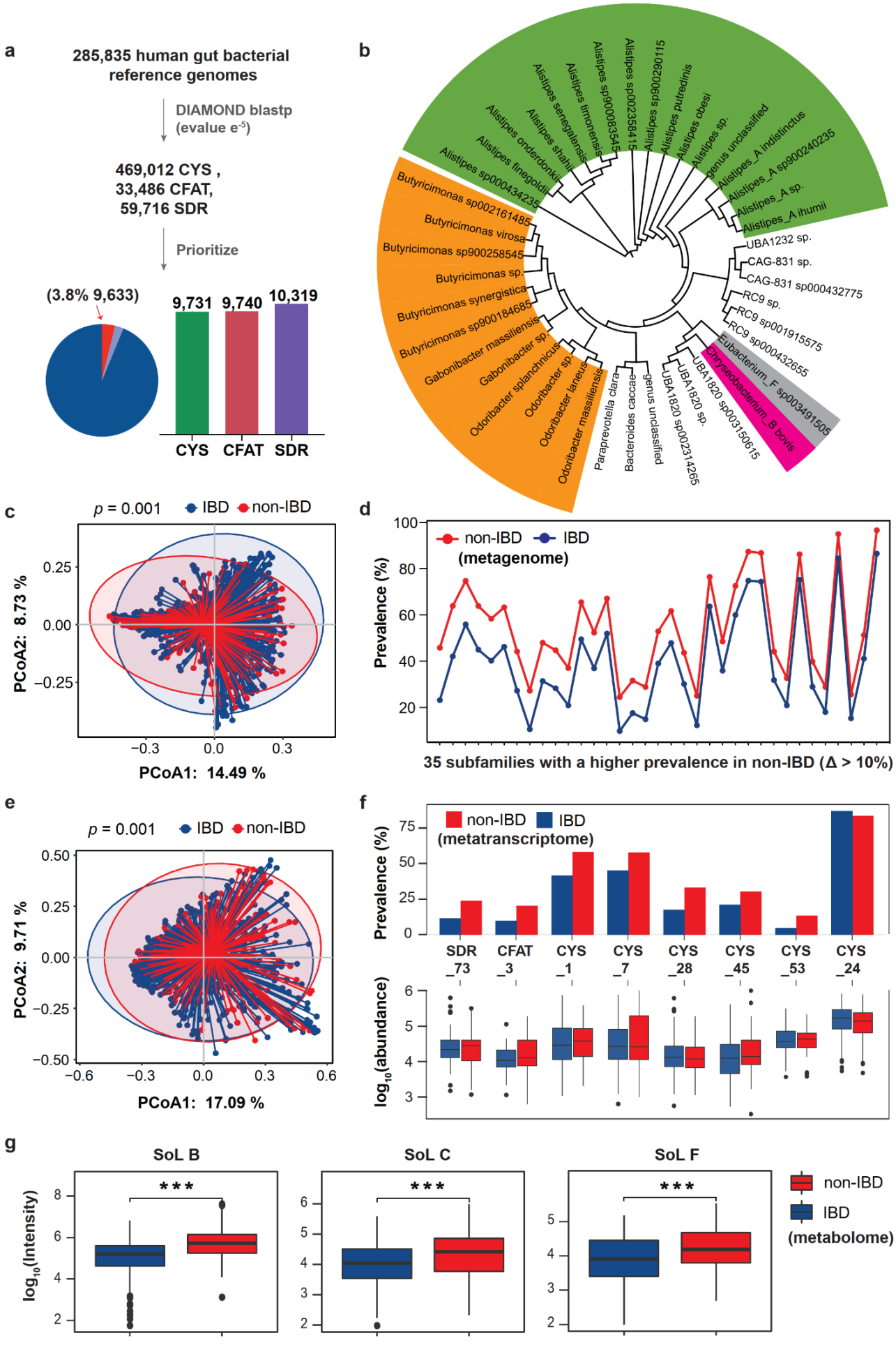
a
285,835 human gut bacterial reference genomes
DIAMOND blastp (evalue e-5)
469,012 CYS , 33,486 CFAT, 59,716 SDR
Prioritize
(3.8% 9,633)
9,731
9,740
10,319
CYS
CFAT
SDR
b
Alistipes sp002358415
Alistipes sp900290115
Alistipes putredinis
Alistipes obesi
Alistipes sp.
genus unclassified
Alistipes_A indistinctus
Alistipes_A sp900240235
Alistipes_A sp.
Alistipes_A ihumii
Alistipes sp000834545
Alistipes timonensis
Alistipes senegalensis
Alistipes shahii
Alistipes onderdonkii
Alistipes finegoldii
Alistipes sp000434235
Butyricimonas sp002161485
Butyricimonas virosa
Butyricimonas sp900258545
Butyricimonas sp.
Butyricimonas synergistica
Butyricimonas sp900184685
Gabonibacter massiliensis
Gabonibacter sp.
Odoribacter splanchnicus
Odoribacter sp.
Odoribacter laneus
Odoribacter massiliensis
Paraprevotella clara
Bacteroides caccae
genus unclassified
UBA1820 sp002314265
UBA1820 sp.
UBA1820 sp003150615
Eubacterium_F sp003491505
Chryseobacterium_B bovis
RC9 sp000432655
RC9 sp001915575
RC9 sp.
CAG-831 sp000432775
CAG-831 sp.
UBA1232 sp.
c
p = 0.001
IBD
non-IBD
PCoA2: 8.73 %
PCoA1: 14.49 %
d
non-IBD
IBD
(metagenome)
Prevalence (%)
35 subfamilies with a higher prevalence in non-IBD (Δ > 10%)
e
p = 0.001
IBD
non-IBD
PCoA2: 9.71 %
PCoA1: 17.09 %
f
non-IBD
IBD
(metatranscriptome)
Prevalence (%)
SDR_73
CFAT_3
CYS_1
CYS_7
CYS_28
CYS_45
CYS_53
CYS_24
log10(abundance)
g
SoL B
SoL C
SoL F
log10(Intensity)
***
non-IBD
IBD
(metabolome)

Fig. 1. The presence and expression profiles of SoL biosynthetic enzymes and the production of SoLs differ in IBD subjects versus healthy controls. a, Overview of SoL biosynthetic enzymes identified in human gut bacteria. 562,214 putative SoL biosynthetic enzymes were identified across 21 bacterial phyla. 6.21% of genomes encode 3 types of SoL biosynthetic enzymes (Pie chart, sections in red and purple). Bar chart shows the number of prioritized SoL biosynthetic enzymes encoded by 9,633 genomes (highlighted in red in the pie chart). **b**, A circular phylogenetic tree shows the prioritized SoL biosynthetic enzymes found primarily in species from Bacteroidota (highlighted in green and orange). The tree is annotated with species names and colored by taxonomic families (*Rikenellaceae*: green; *Marinifilaceae*: orange; *Weeksellaceae*: pink; *Lachnospiraceae*: grey). **c**, Principal Coordinate Analysis (PCoA) shows differences in the presence profile of overall SoL biosynthetic enzyme subfamilies between IBD and non-IBD groups based on Jaccard distance. **d**, 35 SoL biosynthetic enzyme subfamilies were significantly more prevalent in healthy individuals (red dots) than in IBD groups (blue dots) (two-sided Fisher's exact test, $p < 0.05$) with difference of prevalence > 10%. **e**, PCoA showing the differences in the expression profile of overall SoL biosynthetic enzyme subfamilies between IBD and non-IBD groups based on Bray-Curtis distances. **f**, Expression profiles of 8 differential SoL biosynethetic enzyme subfamilies (two-sided Mann-Whitney *U* test, adjusted $p < 0.05$). Upper panel: bar charts showing the prevalence of differential SoL biosynthetic enzyme subfamilies across non-IBD (red) and IBD individuals (dark blue). Statistical significance for prevalence was calculated using a two-sided Fisher's exact test. Except CYS subfamily24 (no significance), all were significantly higher in prevalence in non-IBD than IBD groups ($p < 0.05$). Lower panel: box plots displaying the abundance profiles of differential SoL biosynthetic enzyme subfamilies in non-IBD (red) and IBD individuals (dark blue). Significance was further determined by one-sided Mann-Whitney *U* test, with adjusted *p*-value < 0.05. **g**, Box plots showing the absolute intensity of SoLs B, C, and F detected in non-IBD and IBD individuals collected from IBDMDB. Significance was determined by Wilcoxon rank sum test: * $0.01 < p < 0.05$, ** $0.001 < p < 0.01$, and *** $p < 0.001$.

A mouse study confirms the negative correlation between SoLs production and IBD progression. Encouraged by our informatically predicted negative correlation between SoL biosynthesis and abundance with IBD, we sought to experimentally validate our prediction using a mouse model of IBD. We used a well-

established model of *Il10*-deficient (*IL10*$^{-/-}$) mice treated with the non-steroidal anti-inflammatory drug piroxicam, which has been shown to accelerate development of colitis through the disruption of the gut mucosal barrier[28,29]. Stimulation of mucosal Toll-like receptors (TLRs) stemming from this mucosal barrier breakdown was another factor in our selection of this model, as we have previously shown that SoL A suppresses LPS-induced inflammation and LPS is a well-known TLR signaling molecule[15,30]. Accordingly, we successfully established the piroxicam/*IL10*$^{-/-}$ IBD model and observed that the colonic tissues were inflamed in the piroxicam-treated (IBD) group when compared to the control (pre-IBD) group as indicated by marked crypt hyperplasia, loss of goblet cells, submucosal edema, and immune cell infiltration into the lamina propria (**Fig. 2a**). Gross pathology analysis including qualitative evaluations of cecal atrophy, thickening of cecal and colon tissues, extent of content loss in the cecum, and diarrhea supported induction of IBD with piroxicam treatment (**Fig. 2b, Supplementary Table 5**).

To explore the link between SoLs production and IBD, we collected fecal material from IBD *Il10*$^{-/-}$ + piroxicam (n = 7, female) and pre-IBD control *Il10*$^{-/-}$ mice (n = 4, female)**,** directly extracted SoLs, and measured their abundance by HPLC-HRMS (**Fig. 2c**). We detected metabolites with *m/z* corresponding to major SoLs, specifically SoLs A and B, in all samples tested and unambiguously determined their identities by HPLC-MS/MS (**Fig. 2d**). We then determined that the abundances of both SoLs A and B were significantly decreased in piroxicam treated samples compared to *Il10*$^{-/-}$ control samples (**Fig. 2e, f**). This result confirms our above described informatic analysis and directly establishes a negative correlation between SoLs production and IBD progression in the mouse model. In addition, we also observed significantly increased expression of the NF-κB-regulated inflammatory markers TNFα and NOS2 in the IBD mouse group (Mann-Whitney U test, $p \leq 0.005$; **Fig. 2g, h**), further indicating a negative correlation between SoL production and these inflammatory markers. Given our previously observed anti-inflammatory activity of SoL A against LPS[15], a natural ligand of TLR4, this negative correlation suggests a potential role of SoLs in regulating IBD that may involve suppressing TLR4-mediated NF-κB activation. To eliminate any differences caused by sex, we performed another independent study with male mice using the same IBD model and observed the same negative correlation between SoLs production and IBD progression (**Supplementary Fig. 4**).

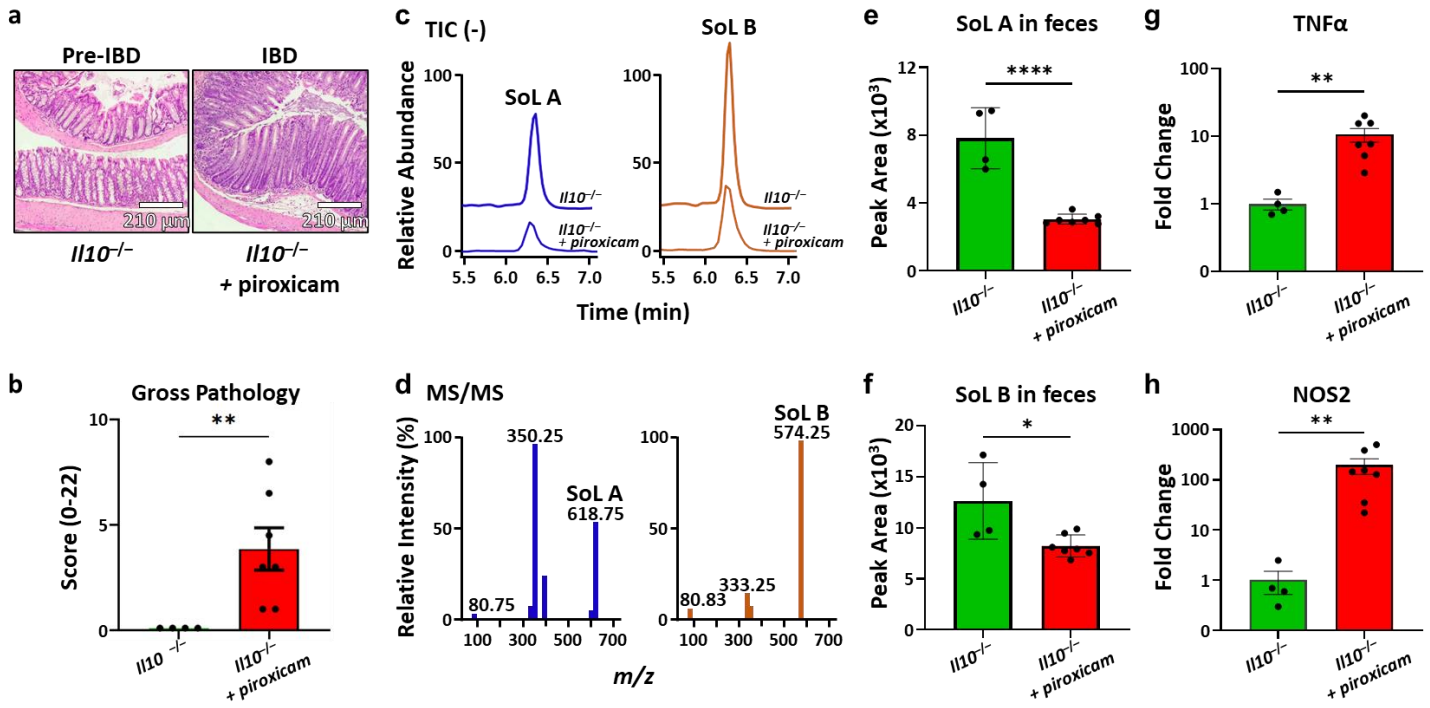

Fig. 2. SoLs are decreased in a mouse model of IBD concurrent with increased concentration of inflammatory markers. a, Histological analysis of the mouse distal colon reveals that piroxicam treatment induced intestinal inflammation. **b**, Overall gross pathology score indicates induction of IBD in *Il10*$^{-/-}$ mice treated with piroxicam (n = 7, female) compared to pre-IBD control *Il10*$^{-/-}$ mice (n = 4, female), confirming the successful establishment of IBD model. The trends were consistent in male mice in another independent experiment using the same IBD model (**Supplementary Fig. 4**). **c**, Total ion chromatograms (TICs) obtained from HPLC-HRMS analysis of fecal pellet extracts from *Il10*$^{-/-}$ and *Il10*$^{-/-}$ + piroxicam mice reveal the presence of SoL A and SoL B. SoL abundances appear to be decreased in abundance in *Il10*$^{-/-}$ + piroxicam mice fecal pellets. **d**, MS/MS spectra of SoLs A and B confirm their identities based on the presence of the 80 *m/z* fragment characteristic of sulfonate-containing compounds and compared to literature fragmentation patterns[11,15]. **e** and **f**, Peak areas were calculated using TICs obtained after MS/MS fragmentation and used to measure the abundance of SoLs A and B. Both SoLs A and B were significantly decreased in mice IBD samples. Significance was determined using Student's *t*-test. **g** and **h**, Expression of inflammatory markers TNFa and NOS2 were significantly increased in *Il10*$^{-/-}$ + piroxicam mice. Significance was determined using Mann-Whitney *U* test. Bars represent mean ± standard error. For all *p* values: ** $0.001 < p < 0.01$ and **** $p < 0.0001$.

Constant identification of SoLs' contribution to immunomodulatory activity. We next examined the production of SoLs and its contribution to immunomodulatory activity in different human gut commensals. Unlike *C. gleum* F93 DSM 16776, which we experimentally investigated for its functional metabolites in relation to inflammatory activity[15], the prolific SoL-producers *Alistipes* and *Odoribacter* had not yet been thoroughly chemically investigated to identify the biologically active components associated with remediation of IBD. In addition, *Alistipes* and *Odoribacter* produce a mixture of other SoLs[11] and are likely to produce a multitude of other functional metabolites, both of which may complicate the potential immunomodulatory activity of these genera's metabolites with respect to their bioinformatically predicted negative association with IBD. Thus, we conducted comparative bioactivity-guided fractionation of 3 *Alistipes* and 2 *Odoribacter* strains (**Supplementary Table 6**) to track the constant contributor(s) to biological activity. We fractionated crude extracts of the *Alistipes* and *Odoribacter* strains and determined the biological activity of each fraction using a cell-based assay which measured the suppression of LPS-indued TNFα production as a metric. We consistently identified SoLs as a major contributor in the active fractions, and multiple rounds of bioactivity-guided purification led to the repeated isolation of SoLs (**Supplementary Fig. 5**). To exclude the possibility of observed SoL activity being influenced by LPS contamination, we confirmed the absence of leftover LPS in the SoL samples using a chromogenic LAL assay (**Supplementary Fig. 6**). By narrowing down the immunosuppressive activity of each of the strains to SoLs, we reinforced the contribution of this class of lipids to the observed biological activity of the *Alistipes* and *Odoribacter* strains.

SoL A mediates dual immunomodulatory activity through TLR signaling. While the causes of IBD remain largely unknown, IBD progression has been linked to aberrant TLR signaling[30]. TLRs are pattern recognition receptors (PRRs) which initiate a variety of host processes, especially inflammatory responses, through the recognition of pathogen-associated molecular patterns (PAMPs) and other non-pathogenic microbial factors[30–32]. Specifically, TLR2 and TLR4 are well-known to recognize PAMPs in the gut microbiome[30]. In addition, their expression is significantly increased in IBD pathogenesis, reflecting a state of aberrant activation[30,32]. Thus, we expected that SoLs may interact with TLR4 or TLR2 to mediate their immunomodulatory activity. We treated primary mouse macrophages with SoL A (as a representative of SoLs) either alone or together

with LPS (an agonist of TLR4) or Pam3CSK4 (an agonist of TLR2) and measured the expression of three inflammatory cytokines (IL-6, TNFα, and IL-1β). By itself, SoL A exhibited a mild to moderate effect on the expression of pro-inflammatory cytokines compared to control (**Fig. 3**), generally consistent with our previous findings[15]. As expected, the TLR ligands, LPS and Pam3CSK4, both showed significant induction of all three cytokines compared to control (Student's *t* test, $p \leq 0.0001$) (**Fig. 3**). Interestingly, SoL A was found to significantly suppress the expression of all three cytokines induced by LPS ($p \leq 0.0001$). SoL A inhibited Pam3CSK4-induced IL-6 and TNFα to a smaller extent while significantly increasing IL-1β expression induced by Pam3CSK4 ($p \leq 0.05$) (**Fig. 3**). This result indicates that SoL A primarily affects LPS-induced inflammation and implies that interaction with TLR4 may be involved in SoL A's mechanism of action. Interestingly, SoL A's partial suppression of Pam3CSK4-induced inflammation suggests that SoL A-related anti-inflammatory activity may also extend to the TLR2 pathway, albeit to a lesser extent, and warrants further investigation.

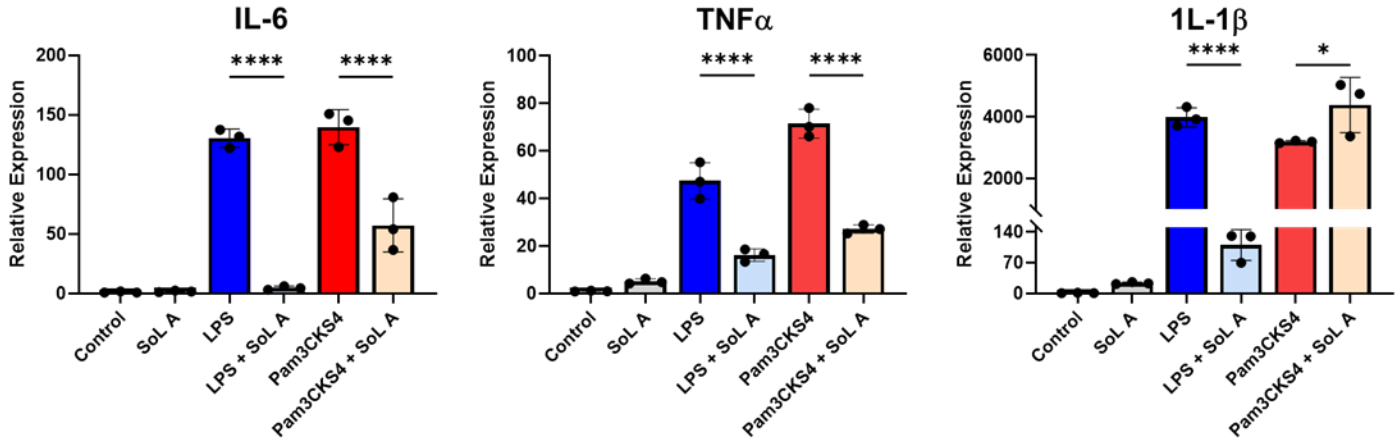

Fig. 3: SoL A primarily suppresses LPS-induced TLR4 activation. Mouse peritoneal primary macrophages were treated with SoL A (10 μM), LPS (50 ng/mL), and Pam3CSK4 (500 ng/mL), either alone or in combination for 6 hours. RT-qPCR analysis revealed that SoL A induces a mild pro-inflammatory effect compared to control but significantly suppresses LPS-induced cytokine expression levels and only partially suppresses Pam3CSK4-induced cytokine expression. Bars represent mean ± standard error. For each treatment, $n = 3$. Significance was determined using Student's *t* test: * $p < 0.05$, **** $p < 0.0001$.

Molecular docking and ELISA displacement assay suggest SoL A binding to TLR4/MD-2 complex. LPS stimulation of TLR4 occurs through a series of interactions ultimately resulting in LPS binding to MD-2, which forms a complex with TLR4 and induces dimerization to initiate signaling[33–35]. The TLR4/MD-2

heterodimer recognizes structurally diverse LPS molecules, giving it flexibility to detect different LPS-related PAMPs in the human gut microbiome[35]. Interestingly, the TLR4/MD-2 complex was recently found to recognize human sulfatides, sphingolipid derivatives which bear a sulfated saccharide head group and dual acyl chains, presumably mimicking the disaccharide core and multiple acyl chains of LPS[36]. Comparing the chemical structure of SoL A to those of sulfatides and lipid A (the immunogenic portion of LPS) (**Fig. 4a**), we noted structural similarity in the negatively charged head groups and multiple acyl chains. We thus considered if multiple molecules of SoL A might bind to MD-2 in a similar configuration as sulfatides and lipid A. Inspired by sulfatides that bind in triplicate to MD-2, we used molecular docking to model the binding of three molecules of SoL A to MD-2. Our analysis predicted three molecules of SoL A indeed bind in the hydrophobic pocket of MD-2, where lipid A is known to bind, with a docking score of -8.9 kcal/mol, better than that of lipid A which had a docking score of -6.2 kcal/mol. Additionally, SoL A was predicted to make hydrophobic contacts with several amino acids including I117, F119, I52, and F121 (**Fig. 4b, Supplementary Table 7**), all of which are also reported to contact the acyl chains of lipid A[35]. Notably, SoL A is also predicted to contact residues including R264 and R90 (**Fig. 4b, Supplementary Table 7**) consistent with contacts between these residues and the phosphate groups of lipid A[35]. This suggests that SoL A may bind directly to the TLR4/MD-2 complex and possibly compete for binding with LPS, allowing it to suppress LPS-induced activation of the TLR4 pathway. A critical aspect of lipid A binding to MD-2 is the exclusion of one acyl chain from the hydrophobic pocket of MD-2 which forms a bridge with TLR4 and is involved in inducing dimerization[35]. Likewise, we observed one acyl chain of SoL A excluded from the hydrophobic pocket in our docking analysis (**Fig. 4b**), further suggesting that SoL A mimics LPS as a ligand for TLR4.

To experimentally determine if SoL A binds to MD-2 and to what extent SoL A competes with LPS for binding to MD-2, we conducted an ELISA-based displacement assay. Taking advantage of biotinylated LPS, which retains the activity of unconjugated LPS[37], we used the fluorescence generated from an HRP-linked streptavidin probe to measure the relative amount of MD-2 which was bound with biotin-LPS as opposed to MD-2 bound with SoL A. We administered 0.1, 1.0, and 10 μM concentrations of SoL A and 1 ng/mL biotin-LPS to MD-2 in three sequences: 1) SoL A first followed by LPS 1 hour later, 2) LPS first followed by SoL A 1 hour

later, and 3) both SoL A and LPS at the same time. After 1 hour of incubation, we found that at all concentrations of SoL A, when SoL A was added first, there was a marked decrease in percent absorbance as compared to when LPS was added first and when the two compounds were added together (**Fig. 4c**). This suggests that SoL A binds and occupies some sites of MD-2, preventing LPS from fully binding when it is added 1 hour after SoL A. Furthermore, when moving from low to high concentrations of SoL A, we observed the percent absorbance decrease dramatically. This indicates that with increasing concentration of SoL A, less LPS binds to MD-2, implying that SoL A indeed competes with LPS for binding to MD-2. Taken together, these results indicate that SoL A can bind directly to MD-2 and also competes with LPS for binding to this target, which provides a molecular mechanism underlying SoL A's pro-inflammatory activity by itself as well as its strong activity in suppressing LPS-induced inflammation.

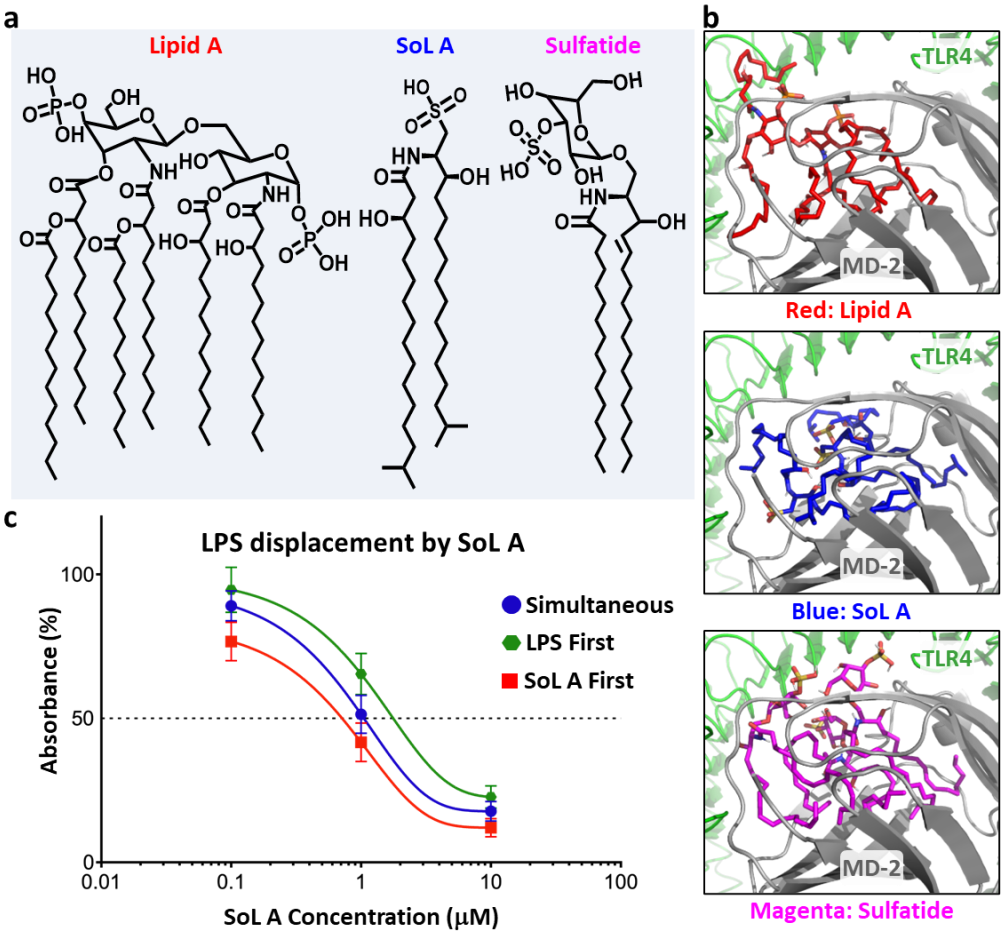

Fig. 4: SoL A bears structural similarity to lipid A and binds with MD-2 to block LPS binding. a, Chemical structures of immunogenic lipid A, derived from LPS, SoL A, and sulfatide illustrating structural similarity in multiple acyl chains and negatively charged head groups. **b**, Molecular docking of lipid A (upper, red) and SoL

A (lower, blue) into the hydrophobic pocket of MD-2 in complex with TLR4. Three molecules of SoL A were used in molecular docking experiments to mimic the six acyl chains of lipid A as inspired by sulfatides[36]. **c**, ELISA displacement assay used to measure the binding behavior of SoL A in competition with LPS, a natural ligand of the TLR4/MD-2 complex. Compounds were added either simultaneously (blue), LPS first (green), or SoL A first (red).

SoL A suppresses LPS-induced TLR4-downstream signaling pathways. Upon LPS binding, TLR4 initiates downstream signaling, such as through the NF-kB and MAPK pathways, resulting in the induction of inflammatory cytokine expression[32]. If SoL A binds to MD-2 to suppress LPS-induced inflammation, this would block activation of the TLR4 pathway. Therefore, we investigated whether addition of SoL A affected the phosphorylation of TLR4-downsteam signaling molecules, ATF-2 and p38, and the degradation of IκBα, which are critical for LPS-induced cytokine expression[32] (**Fig. 5a**). We treated macrophages with LPS in the presence of increasing concentrations of SoL A (from 0 to 20 μM), then performed western blot analysis to examine the TLR4-downstream signaling pathways. We found that SoL A reduced LPS-induced phosphorylation of p38 and ATF2 in a concentration-dependent manner. At the concentration of 20 μM, Sol A almost completely blocked LPS-induced phosphorylation of p38 and ATF2 (**Fig. 5b**). Western blot also showed that Sol A concentration-dependently suppressed LPS-induced IκBα degradation (**Fig. 5b**). These results support that SoL A exerts its anti-inflammatory effect by blocking LPS-mediated phosphorylation of downstream TLR4 proteins, effectively negating LPS activation of the TLR4 pathway. Notably, SoL A alone at the highest concentration had little effect on the proteins tested compared to control, despite our previous observation that SoL A induced a mild pro-inflammatory effect. This suggests that in addition to targeting TLR4, SoL A may also exert its pro-inflammatory effect via other pathways such as TLR2 which we described above (**Fig. 3**), providing further opportunities to explore this complex activity.

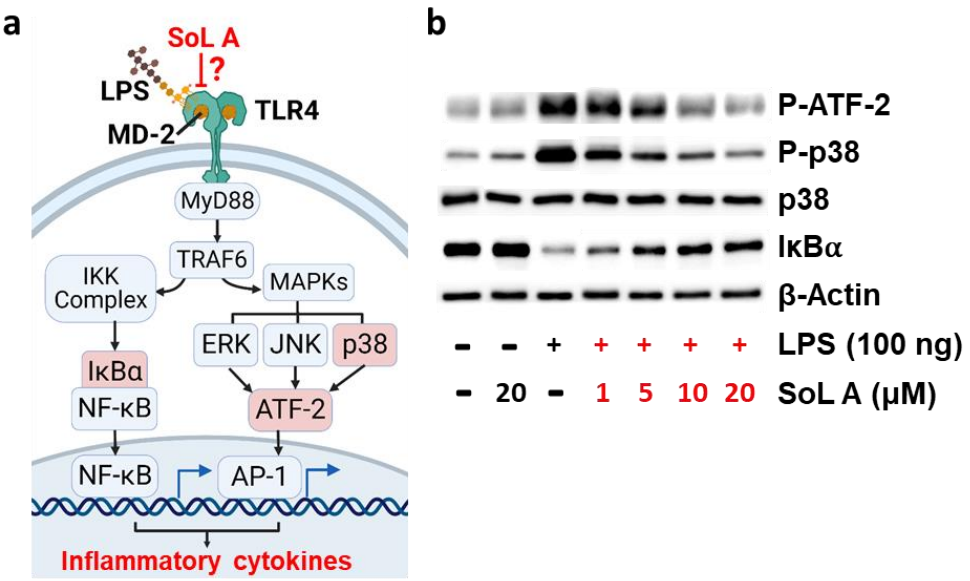

Fig. 5: SoL A suppresses LPS-induced activation of TLR4 signaling pathway. a, Simplified pathway of TLR4 activation by LPS highlighting proposed inhibition by SoL A competing for LPS binding. Proteins IκBα, p38, and ATF-2 downstream of TLR4 which were selected for analysis are highlighted in red rectangles. **b**, Western blot analysis of total protein concentration of ATF-2, p38, and IκBα after treatment with SoL A, 100 ng LPS, or 100 ng LPS with 1, 5, 10, or 20 μM SoL A. The housekeeping gene β-Actin was used as a loading control.

Discussion

The results of this study have described two critical points, briefly summarized here and discussed in further detail below. First, we have leveraged multi-omics bioinformatic and chemoinformatic analyses to directly connect the biosynthesis and production of a class of abundant human microbial metabolites, SoLs, to IBD, an existing human health condition with complex and poorly understood etiology and further use a mouse model of IBD to validate our informatic predictions. Second, we have revealed that SoL A, as a representative of SoLs, modulates host immune responses through the TLR4/MD-2 complex and inhibits LPS-induced TLR4 activation.

Through informatic analysis, we revealed that the expression of SoL biosynthetic genes and abundance of SoLs in the gut metabolome are negatively correlated with IBD. Our IBD model with piroxicam treated *Il10*$^{-/-}$ mice supported this negative correlation in addition to a concurrent negative association of SoLs production with TLR-4-related inflammatory markers such as TNFα and NOS2. While many studies have focused on association

of certain microbial strains with specific diseases by analyzing the abundance and distribution of strains[7,8,38–41], our results have shown that the presence and expression of biosynthetic enzymes corresponding to functional metabolites can be directly correlated with human health conditions, effectively shifting the microbe-focused perspective to a functional metabolite-based molecular perspective. Applying this approach, our findings were consistent with literature reports which have shown that the SoL-producing bacterial genera, *Alistipes* and *Odoribacter*, are also associated with the remediation of IBD symptoms[9,10]. Considering that these SoL producers are commensal members of the human gut microbiome[11,42], their constant production of SoLs in the human gut may help to maintain intestinal immune homeostasis, thus preventing IBD. Both *Alistipes* and *Odoribacter* are also known to produce short chain fatty acids (SCFAs), which have also been implicated in reducing intestinal inflammation[10,42–45]. Besides SCFAs, there are many other gut microbial functional metabolites such as secondary bile acids and indole derivatives which have been linked to modulating host inflammation and immunity[46–48]. Thus, the specific role SoLs play in IBD pathogenesis and whether they act alone or in combination with other factors remain interesting open questions.

Towards understanding the mechanism of the dual immunomodulatory activity of SoL A, we showed that SoL A primarily targets the TLR4 pathway and likely competitively binds to MD-2 to mediate suppression of TLR4 activation. Our analysis indicated that SoL A preferentially suppresses LPS-induced inflammation as compared to Pam3CSK4-induced inflammation, suggesting that TLR4 activation is more strongly affected by SoL A than TLR2 activation. The selectivity for TLR4 may stem from SoL A's structural similarity to LPS, a hypothesis supported by the recently reported human TLR4 ligands, sulfatides, which also share highly similar structural features to SoL A[36]. As a microbial functional metabolite, it is reasonable that SoL A is directly recognized by TLR4, which has evolved specifically to recognize PAMPs. Our molecular docking also suggested SoL A's recognition by TLR4, indicating that three molecules of SoL A indeed bind with stronger predicted binding score and make contacts with important amino acids in the pocket of MD-2, consistent with lipid A binding as well as structurally-related sulfatides[35,36]. Our ELISA-based displacement analysis then confirmed that SoL A directly binds to MD-2, blocks LPS binding when added prior to LPS, and could also displace bound LPS from MD-2 at higher concentrations. We further demonstrated that increasing concentration of SoL A suppressed

LPS-induced TLR4-downstream signaling pathways in a dose-dependent manner. Taken together, our results represent the first report of SoL A's direct binding to MD-2 and establish that SoL A mediates its dual immunomodulatory activity by blocking LPS binding to the TLR4/MD-2 complex. This discovery suggests SoL A's role in regulating a multitude of TLR4-related inflammatory conditions, most notably IBD which is associated with increased expression of TLRs, especially TLR4[16–19]. By applying our functional metabolite-focused approach, we have identified a potential explanation for the protective effect that SoL-producing bacteria exert against IBD. We expect this approach to be applicable to uncovering the molecular mechanisms of other intricate host-microbe interactions.

Methods

Identification of SoL biosynthetic enzymes from human gut bacterial reference genomes. We collected experimentally validated enzymes involved in SoL biosynthesis as reference amino acid sequences of CYS, CFAT, and SDR (**Supplementary Table 1**). Reference amino acid sequences were used as seed sequences to search for homologs in the human gut bacterial reference genomes using the DIAMOND blastp model[49] with an e-value threshold of 10^{-5}. We then investigated the taxonomic distribution of the resulting homolog sets based on the taxonomy annotation for each genome[20]. To prioritize SoL biosynthetic enzymes, the homologs of CFATs and CYSs from genomes which encode copies of CFAT, CYS and SDR were first used to generate sequence similarity networks with experimentally validated CFAT and CYS at a threshold of 50% similarity using MMseqs2[50]. The prioritized CFATs and CYSs meet co-occurrence with SDRs in the same genome. The filtered enzymes were further subjected to Pfam domain analysis by hmmsearch (HMMER v3.3) with default parameters against the Pfam-A database (v33.1). Enzymes containing corresponding Pfam domains with hit score > 50 were selected as prioritized SoL biosynthetic enzymes. Prioritized enzymes were used to generate CYS, CFAT, and SDR subfamilies using sequence similarity networks with at least 90% similarity by MMseqs2 clustering[50]. Maximum-likelihood trees were generated using the representative genome of each species by GTDB-Tk (v2)[51]. Finally, we selected a representative genome for each species to display their SoL biosynthetic potential and annotate their phylogenetic trends using iTOL[52].

Quantification of enzyme abundances in metagenomic and metatranscriptomic samples. Metagenomic and metatranscriptomic whole-genome sequencing datasets of human gut microbiomes related to IBD were downloaded from the NCBI Sequence Read Archive (SRA) (SRA Accessions: PRJNA398089 and PRJNA389280*).* For both metagenomic and metatranscriptomic samples, reads were quality filtered and adapter removed using *bbduk.sh* with the following parameters: qtrim=rl ktrim=r mink=11 trimq=10 minlen=40 (read quality cutoff is 10, read length cutoff is 40). High-quality reads were mapped to the nucleotide sequences of corresponding contigs containing the SoL biosynthetic genes using BWA mem algorithm[53] with default parameters. The reads mapped to genes were counted by featurecounts[54] with the following parameters: -f -t CDS -M -O -g transcript_id -F GTF -s 0 -p --fracOverlap 0.25 -Q 10 –primary. Enzymes encoded or expressed in at least 5% of samples were considered as common distribution in humans and were included in the comparative analysis. Transcripts per million (TPM) were calculated for each SoL biosynthetic enzyme gene. The abundance of each cluster was calculated by the sum of the relative abundances of all genes in the cluster. Beta diversity was performed to quantify the prevalence and relative abundance differences in the overall composition of SoL biosynthetic enzymes between the IBD and the control groups. PERMANOVA was performed to show the encoding and expression profile differences of SoL biosynthetic enzymes between IBD and control groups. Both beta diversity and PERMANOVA were performed using the R package vegan[55,56]. To explore the differences between IBD and control groups of single SoL biosynthetic enzyme subfamilies, we used the Shapiro–Wilk test to evaluate the normality of a specific gene cluster's relative abundance. We then calculated the significance of relative abundance between healthy and IBD individuals using either two-sample Student's t-test (for normally distributed data) or two-sample Wilcoxon rank sum test (for not normally distributed data). Significance tests were performed in Python using packages Pandas and SciPy[57–59]. The Benjamini-Hochberg method was used to adjust p-values to correct for multiple testing[60]. SoL biosynthetic enzyme subfamilies was considered a differential gene cluster if the adjusted p-value was less than 0.05. For differential Sol biosynthetic enzymes, we performed a two-sided Fisher's exact test to explore their difference in prevalence across IBD and non-IBD groups.

Analysis of publicly available metabolomics datasets. Two publicly available metabolomics datasets were downloaded from IBDMDB (https://ibdmdb.org/tunnel/public/summary.html) and Metabolomics Workbench (http://www.metabolomicsworkbench.org). Processed metabolomic feature tables were used to search for SoL related metabolites (sulfobacins A-F). Search parameters were set to the exact mass of sulfobacins A-F using a 5ppm match tolerance for parent ions under negative mode. The absolute intensity of relative abundance from resulting matches were used to calculate differential abundances between non-IBD and IBD samples. Wilcoxon signed-rank test was used to measure statistical significance.

Animals. *Il10*$^{-/-}$ mice were originally purchased from The Jackson Laboratory. Mice were maintained in specific pathogen free conditions at the University of South Carolina and were maintained on a 12-hour light/dark cycle with unlimited access to water and food (Envigo 8904). All animal protocols were approved by the University of South Carolina Institutional Animal Care and Use Committee.

Piroxicam-accelerated *Il10*$^{-/-}$ mouse IBD model and analysis. At 8-12 weeks of age, male and female *Il10*$^{-/-}$ mice (n = 7 per sex) were switched to a diet containing 100 ppm of piroxicam (Sigma) (Envigo, TD.210442) to induce colitis development as previously described[29]. Male (n = 3) and female (n = 4) *Il10*$^{-/-}$ mice were maintained on the control diet for the duration of the experiment to serve as pre-IBD controls. Mice were euthanized at 18 days to collect tissues for assessment and intestinal contents for quantification of SoLs. At necropsy, IBD severity was first grossly assessed, which included qualitative evaluations of cecal atrophy (0–5), thickening of cecal (0–5) and colon tissues (0–5), extent of content loss in the cecum (0–4) and diarrhea (0–3). For histopathology, segments of the colon were first washed in PBS and then fixed in 10% neutral buffered formalin. The tissues were embedded in paraffin, cut into 5-mm sections, and stained with hematoxylin and eosin (H&E) at the Instrumentation Resource Facility at the University of South Carolina School of Medicine. Inflammation scores of colon sections were blindly assessed as previously described[61] using an Echo Revolve light microscope and accompanying software. Briefly, IBD severity was assessed based on the following histopathological features: length measurements in microns of crypt hyperplasia converted to a score from 0-4, qualitative assessment of goblet cell loss (0–5), crypt abscesses per 10X field counts converted to a score from 0-4, and qualitative assessment of submucosal edema (0-3). RNA isolations and RT-qPCR were performed as

previously described[62]. Briefly, RNA was isolated from snap frozen colon tissues using the TriZol method (Thermo Fisher Scientific). cDNA was synthesized using SuperScript III reverse transcriptase (ThermoFisher Scientific). qRT-PCR was performed at the Functional Genomics Core at the University of South Carolina. The relative abundance of mammalian mRNA transcripts was calculated using the delta delta CT method and normalized to *Eef2* levels. The oligonucleotides used for qRT-PCR were: *Eef2* forward: TGTCAGTCATCGCCCATGTG, reverse: CATCCTTGCGAGTGTCAGTGA; *Tnfa* forward: AGCCAGGAGGGAGAACAGAAAC, reverse: CCAGTGAGTGAAAGGGACAGAACC; *Nos2* forward TTGGGTCTTGTTCACTCCACGG, reverse: CCTCTTTCAGGTCACTTTGGTAGG. Fecal samples were collected and immediately flash frozen and stored at -80 C. For SoL extraction and quantification, frozen fecal samples were lyophilized to remove remaining water and subsequently resuspended in methanol (ThermoFisher Scientific). Fecal sample suspensions were vortexed for 1 minute prior to sonication for 10 minutes. The methanol extract was collected by centrifugation at 20,000 x *g* for 10 minutes and dried under a gentle stream of nitrogen. The resulting residue was then redissolved in methanol + 0.1% ammonium hydroxide (ThermoFisher Scientific) and filtered through a 0.22 μm filter prior to analysis. High-resolution mass spectra were collected using a ThermoFisher Scientific Q-Exactive HF-X hybrid Quadrupole-Orbitrap mass spectrometer using electrospray ionization in negative mode. Liquid chromatography used a ThermoFisher Scientific Vanquish HPLC coupled to the aforementioned mass spectrometer. LC was performed using a Waters Xbridge BEH C18 XP column (2.1 x 100 mm) with mobile phases A: water + 0.1% ammonium hydroxide, and B: acetonitrile + 0.1% ammonium hydroxide in a gradient starting from 10% B and increasing to 100% B over 5 minutes, hold at 100% B for 2.5 minutes, then re-equilibration at 10% B for 2.5 minutes. MS scans were obtained in the orbitrap analyzer which was scanned from 500 to 2000 m/z at a resolution of 60,000 (at 200 m/z). MS data was analyzed by Thermo Xcalibur (4.2.47).

Anaerobic culture and bioactivity-guided isolation of SoL A. Three *Alistipes* and two *Odoribacter* strains (**Supplementary Table 6**) were cultured in Reinforced Clostridial Medium (RCM, BD Biosciences) under anaerobic conditions at 37°C. After three days of growth, cultures were harvested by centrifugation at 12,000 x *g* for 30 minutes. SoLs were extracted and purified as previously described with minor modification[15]. At each step

in the isolation process, biological activity was assessed by measuring the suppression of LPS-induced TNFα production of each fraction. Briefly, the cell-free supernatant was extracted with an equal volume of methyl ethyl ketone while the cell pellet was extracted with methanol and prolonged sonication. The two extracts were re-combined and fractionated by silica gel C18 using a stepwise gradient of methanol and water with 0.1% ammonium hydroxide. Active fractions were further fractionated by Sephadex LH-20 run in 1:1 DCM:MeOH. Finally, pure SoL A was isolated by semi-preparative scale HPLC running an isocratic solvent composition of 65% water with 0.1% ammonium hydroxide and 35% acetonitrile with 0.1% ammonium hydroxide. Purified SoL A was confirmed to be free of LPS using a Chromogenic Endotoxin Quant Kit (Pierce).

Preparation and treatment of macrophages. Primary mouse macrophages were prepared by first introducing 3 mL of 3% thioglycolate to mice via intraperitoneal injection. After 3 days, 10 mL of chilled PBS was introduced intraperitoneally to flush out macrophages. The cell suspension was then separated by centrifugation at 300 x *g* for 5 min. Cells were seeded in culture dishes containing DMEM with 10% FBS for 1 hour before being washed with serum-free DMEM two times to remove unattached cells. To treat the macrophages, cells were incubated for 6 to 24 h in DMEM without FBS with addition of LPS (Sigma-Aldrich), Pam3CSK4 (Invivogen), or SoL A. Cells were finally washed twice with Dulbecco's phosphate-buffered saline before being lysed for total RNA or protein extraction.

mRNA extraction and RT-qPCR in macrophage-based assays. Treated mouse macrophage cells were lysed with TriZol (Invitrogen) and total RNA was extracted from the cell lysate using a Direct-zol RNA miniprep kit (Zymo Research) according to the manufacturer's protocol. The quality and quantity of RNA was then determined using a nanodrop and 1000 ng of mRNA from each sample was used for cDNA synthesis using a First-strand cDNA Synthesis System (Marligen Bioscience). qPCRs reactions were prepared in a 20 uL final volume containing Fast Start Universal SYBR Green Master (Rox) (Roche Applied Science), cDNA template, deionized water, and primers and probes for IL-1β, TNFα, IL-6, and the 18S rRNA which was used as a housekeeping gene Cycling conditions were 95 °C for 10 min followed by 40 cycles of 95 °C for 10 seconds, 60 °C for 15 seconds, and 68 °C for 20 seconds, then a melting curve analysis from 60 °C to 95°C every 0.2 °C was obtained. Amplifications were performed on an Eppendorf Realplex Mastercycler (Eppendorf). Relative gene

expression levels were calculated using the $\Delta\Delta C_T$ method and expression levels of 18S were used to normalize the results.

Molecular docking. The crystal structure of the TLR4/MD-2 comlpex was retrieved from the Protein Data Bank (PDB ID: 3FXI)[35] and prepared using AutoDock Tools[63]. Molecular structures of SoL A and lipid A were constructed, and energy minimized using Marvin version 21.17.0, ChemAxon (https://www.chemaxon.com). Models of SoL A and lipid A were also prepared using AutoDock Tools and docked against the TLR4/MD-2 complex using AutoDock Vina[64,65] in a 32x32x32 angstrom box surrounding the MD-2 monomer. Docking results were visualized using PyMol[66].

ELISA displacement assay. Solid-phase sandwich ELISA kits were purchased from Invitrogen. The ELISA experiments were performed according to the kit instructions, using 50 nM hMD-2 (Novus Biologicals), 1 ng/mL LPS-EB Biotin (Invivogen), and 0.1, 1.0, and 10 μM purified SoL A. SoL A was added to the assay 1 hour before, 1 hour after, or simultaneously with LPS-EB Biotin. Absorbance was measured at 450 nm using a BioTek microplate reader.

Western blot. Macrophages were treated with 50 ng of LPS and 1, 5, 10, and 20 μM SoL A for 30 minutes. Following treatment, all cellular protein was extracted using MPER lysis buffer (Thermo Scientific). Protein samples were loaded onto SDS-PAGE gels for separation, then transferred to nitrocellulose membranes (Amersham Biosciences). Primary antibodies and HRP-conjugated secondary antibodies (Cell Signaling Technology) were used to detect target proteins. Signal was detected using an ECL kit (Thermo Scientific).

References

1. Donia, M. S. & Fischbach, M. A. Small molecules from the human microbiota. *Science* **349**, 1254766 (2015).
2. Quinn, R. A. *et al.* Global chemical effects of the microbiome include new bile-acid conjugations. *Nature* **579**, 123–129 (2020).
3. Lavelle, A. & Sokol, H. Gut microbiota-derived metabolites as key actors in inflammatory bowel disease. *Nat Rev Gastroenterol Hepatol* **17**, 223–237 (2020).

4. Skelly, A. N., Sato, Y., Kearney, S. & Honda, K. Mining the microbiota for microbial and metabolite-based immunotherapies. *Nat Rev Immunol* **19**, 305–323 (2019).
5. Spanogiannopoulos, P., Bess, E. N., Carmody, R. N. & Turnbaugh, P. J. The microbial pharmacists within us: a metagenomic view of xenobiotic metabolism. *Nat Rev Microbiol* **14**, 273–287 (2016).
6. Brown, E. M., Clardy, J. & Xavier, R. J. Gut microbiome lipid metabolism and its impact on host physiology. *Cell Host & Microbe* **31**, 173–186 (2023).
7. Durack, J. & Lynch, S. V. The gut microbiome: Relationships with disease and opportunities for therapy. *Journal of Experimental Medicine* **216**, 20–40 (2018).
8. Lloyd-Price, J. *et al.* Multi-omics of the gut microbial ecosystem in inflammatory bowel diseases. *Nature* **569**, 655–662 (2019).
9. Dziarski, R., Park, S. Y., Kashyap, D. R., Dowd, S. E. & Gupta, D. Pglyrp-regulated gut microflora *Prevotella falsenii*, *Parabacteroides distasonis* and *Bacteroides eggerthii* enhance and *Alistipes finegoldii* attenuates colitis in mice. *PLOS ONE* **11**, e0146162 (2016).
10. Lima, S. F. *et al.* Transferable immunoglobulin A–coated *Odoribacter splanchnicus* in responders to fecal microbiota transplantation for ulcerative colitis limits colonic inflammation. *Gastroenterology* **162**, 166–178 (2022).
11. Walker, A. *et al.* Sulfonolipids as novel metabolite markers of *Alistipes* and *Odoribacter* affected by high-fat diets. *Scientific Reports* **7**, 11047 (2017).
12. MacEyka, M. & Spiegel, S. Sphingolipid metabolites in inflammatory disease. *Nature* **510**, 58–67 (2014).
13. Olsen, I. & Jantzen, E. Sphingolipids in bacteria and fungi. *Anaerobe* **7**, 103–112 (2001).
14. Pitta, T. P., Leadbetter, E. R. & Godchaux, W. Increase of ornithine amino lipid content in a sulfonolipid-deficient mutant of *Cytophaga johnsonae*. *J Bacteriol* **171**, 952–957 (1989).
15. Hou, L. *et al.* Identification and biosynthesis of pro-inflammatory sulfonolipids from an opportunistic pathogen *Chryseobacterium gleum*. *ACS chemical biology* **17**, 1197–1206 (2022).

16. Pasternak, B. A. *et al.* Lipopolysaccharide exposure is linked to activation of the acute phase response and growth failure in pediatric Crohn's disease and murine colitis: *Inflammatory Bowel Diseases* **16**, 856–869 (2010).
17. Caradonna, L. *et al.* Invited review: Enteric bacteria, lipopolysaccharides and related cytokines in inflammatory bowel disease: biological and clinical significance. *Journal of Endotoxin Research* **6**, 205–214 (2000).
18. Pastor Rojo, O. *et al.* Serum lipopolysaccharide-binding protein in endotoxemic patients with inflammatory bowel disease. *Inflamm Bowel Dis* **13**, 269–277 (2007).
19. Im, E., Riegler, F. M., Pothoulakis, C. & Rhee, S. H. Elevated lipopolysaccharide in the colon evokes intestinal inflammation, aggravated in immune modulator-impaired mice. *American Journal of Physiology-Gastrointestinal and Liver Physiology* **303**, G490–G497 (2012).
20. Almeida, A. *et al.* A unified catalog of 204,938 reference genomes from the human gut microbiome. *Nat Biotechnol* **39**, 105–114 (2021).
21. Liu, Y. *et al.* Identification and characterization of the biosynthetic pathway of the sulfonolipid capnine. *Biochemistry* **61**, 2861–2869 (2022).
22. Vences-Guzmán, M. Á. *et al.* Identification of the *Flavobacterium johnsoniae* cysteate-fatty acyl transferase required for capnine synthesis and for efficient gliding motility. *Environmental Microbiology* **23**, 2448–2460 (2021).
23. Radka, C. D., Miller, D. J., Frank, M. W. & Rock, C. O. Biochemical characterization of the first step in sulfonolipid biosynthesis in *Alistipes finegoldii*. *The Journal of biological chemistry* **298**, 1–13 (2022).
24. Radka, C. D., Frank, M. W., Rock, C. O. & Yao, J. Fatty acid activation and utilization by *Alistipes finegoldii*, a representative Bacteroidetes resident of the human gut microbiome. *Molecular Microbiology* **113**, 807–825 (2020).
25. Kamiyama, T. *et al.* Sulfobacins A and B, novel von Willebrand factor receptor antagonists: I. Production, isolation, characterization and biological activities. *The Journal of Antibiotics* **48**, 924–928 (1995).

26. Schirmer, M. *et al.* Dynamics of metatranscription in the inflammatory bowel disease gut microbiome. *Nat Microbiol* **3**, 337–346 (2018).

27. Franzosa, E. A. *et al.* Gut microbiome structure and metabolic activity in inflammatory bowel disease. *Nat Microbiol* **4**, 293–305 (2019).

28. Hale, L. P., Gottfried, M. R. & Swidsinski, A. Piroxicam treatment of IL-10-deficient mice enhances colonic epithelial apoptosis and mucosal exposure to intestinal bacteria. *Inflammatory Bowel Diseases* **11**, 1060–1069 (2005).

29. Berg, D. J. *et al.* Rapid development of colitis in NSAID-treated IL-10-deficient mice. *Gastroenterology* **123**, 1527–1542 (2002).

30. Cario, E. Toll-like receptors in inflammatory bowel diseases: A decade later. *Inflammatory Bowel Diseases* **16**, 1583–1597 (2010).

31. Akira, S. & Takeda, K. Toll-like receptor signalling. *Nat Rev Immunol* **4**, 499–511 (2004).

32. Kawasaki, T. & Kawai, T. Toll-like receptor signaling pathways. *Frontiers in Immunology* **5**, 1–8 (2014).

33. Shimazu, R. *et al.* MD-2, a molecule that confers lipopolysaccharide responsiveness on Toll-like receptor 4. *Journal of Experimental Medicine* **189**, 1777–1782 (1999).

34. Miyake, K. Invited review: Roles for accessory molecules in microbial recognition by Toll-like receptors. *Journal of Endotoxin Research* **12**, 195–204 (2006).

35. Park, B. S. *et al.* The structural basis of lipopolysaccharide recognition by the TLR4–MD-2 complex. *Nature* **458**, 1191–1195 (2009).

36. Su, L. *et al.* Sulfatides are endogenous ligands for the TLR4–MD-2 complex. *Proceedings of the National Academy of Sciences of the United States of America* **118**, 1–12 (2021).

37. Luk, J. M., Kumar, A., Tsang, R. & Staunton, D. Biotinylated lipopolysaccharide binds to endotoxin receptor in endothelial and monocytic cells. *Analytical Biochemistry* **232**, 217–224 (1995).

38. Bhattarai, Y., Muniz Pedrogo, D. A. & Kashyap, P. C. Irritable bowel syndrome: A gut microbiota-related disorder? *American Journal of Physiology-Gastrointestinal and Liver Physiology* **312**, G52–G62 (2016).

39. Wang, J. *et al.* A metagenome-wide association study of gut microbiota in type 2 diabetes. *Nature* **490**, 55–60 (2012).

40. Thomann, A. K. *et al.* Depression and fatigue in active IBD from a microbiome perspective-a Bayesian approach to faecal metagenomics. *BMC Med* **20**, 366 (2022).

41. Mars, R. A. T. *et al.* Longitudinal multi-omics reveals subset-specific mechanisms underlying irritable bowel syndrome. *Cell* **182**, 1460-1473.e17 (2020).

42. Parker, B. J., Wearsch, P. A., Veloo, A. C. M. & Rodriguez-Palacios, A. The genus *Alistipes*: Gut bacteria with emerging implications to inflammation, cancer, and mental health. *Frontiers in Immunology* **11**, 906 (2020).

43. Koh, A., De Vadder, F., Kovatcheva-Datchary, P. & Bäckhed, F. From dietary fiber to host physiology: Short-chain fatty acids as key bacterial metabolites. *Cell* **165**, 1332–1345 (2016).

44. Chang, P. V., Hao, L., Offermanns, S. & Medzhitov, R. The microbial metabolite butyrate regulates intestinal macrophage function via histone deacetylase inhibition. *Proc. Natl. Acad. Sci. U.S.A.* **111**, 2247–2252 (2014).

45. Trapecar, M. *et al.* Gut-liver physiomimetics reveal paradoxical modulation of IBD-related inflammation by short-chain fatty acids. *Cell Systems* **10**, 223-239.e9 (2020).

46. Bhattarai, Y. *et al.* Bacterially derived tryptamine increases mucus release by activating a host receptor in a mouse model of inflammatory bowel disease. *iScience* **23**, 101798 (2020).

47. Dodd, D. *et al.* A gut bacterial pathway metabolizes aromatic amino acids into nine circulating metabolites. *Nature* **551**, 648–652 (2017).

48. Paik, D. *et al.* Human gut bacteria produce TH17-modulating bile acid metabolites. *Nature* **603**, 907–912 (2022).

49. Buchfink, B., Reuter, K. & Drost, H.-G. Sensitive protein alignments at tree-of-life scale using DIAMOND. *Nat Methods* **18**, 366–368 (2021).

50. Mirdita, M., Steinegger, M., Breitwieser, F., Söding, J. & Levy Karin, E. Fast and sensitive taxonomic assignment to metagenomic contigs. *Bioinformatics* **37**, 3029–3031 (2021).

51. Chaumeil, P.-A., Mussig, A. J., Hugenholtz, P. & Parks, D. H. GTDB-Tk v2: memory friendly classification with the genome taxonomy database. *Bioinformatics* **38**, 5315–5316 (2022).

52. Letunic, I. & Bork, P. Interactive Tree Of Life (iTOL) v5: an online tool for phylogenetic tree display and annotation. *Nucleic Acids Research* **49**, W293–W296 (2021).

53. Li, H. & Durbin, R. Fast and accurate short read alignment with Burrows–Wheeler transform. *Bioinformatics* **25**, 1754–1760 (2009).

54. Liao, Y., Smyth, G. K. & Shi, W. featureCounts: an efficient general purpose program for assigning sequence reads to genomic features. *Bioinformatics* **30**, 923–930 (2014).

55. R Core Team. *R: A language and environment for statistical computing*. https://www.R-project.org/ (2021).

56. Oksanen, J. *et al. vegan: Community ecology package*. https://CRAN.R-project.org/package=vegan (2020).

57. Van Rossum, G. & Drake, F. L. *Python 3 reference manual*. (CreateSpace, 2009).

58. McKinney, W. & others. Data structures for statistical computing in python. in *Proceedings of the 9th python in science conference* vol. 445 51–56 (2010).

59. Virtanen, P. *et al.* SciPy 1.0: Fundamental algorithms for scientific computing in python. *Nature Methods* **17**, 261–272 (2020).

60. Benjamini, Y. & Hochberg, Y. Controlling the false discovery rate: A practical and powerful approach to multiple testing. *Journal of the Royal Statistical Society: Series B (Methodological)* **57**, 289–300 (1995).

61. Erben, U. *et al.* A guide to histomorphological evaluation of intestinal inflammation in mouse models. *Int J Clin Exp Pathol* **7**, 4557–4576 (2014).

62. Ellermann, M. *et al.* Endocannabinoids Inhibit the Induction of Virulence in Enteric Pathogens. *Cell* **183**, 650-665.e15 (2020).

63. Morris, G. M. *et al.* AutoDock4 and AutoDockTools4: Automated docking with selective receptor flexibility. *J Comput Chem* **30**, 2785–2791 (2009).

64. Trott, O. & Olson, A. J. AutoDock Vina: Improving the speed and accuracy of docking with a new scoring function, efficient optimization, and multithreading. *Journal of Computational Chemistry* **31**, 455–461 (2010).

65. Eberhardt, J., Santos-Martins, D., Tillack, A. F. & Forli, S. AutoDock Vina 1.2.0: New docking methods, expanded force field, and python bindings. *J. Chem. Inf. Model.* **61**, 3891–3898 (2021).

66. Schrödinger, LLC. The PyMOL molecular graphics system, version 2.0. (2015).

Acknowledgements

This work is partially funded by a National Institutes of Health (NIH) grant P20GM103641, a National Science Foundation EPSCoR Program OIA-1655740, a Hong Kong Research Grants Council ECS grant HKU27107320, and the Hong Kong Branch of Southern Marine Science and Engineering Guangdong Laboratory (Guangzhou) (SMSEGL20SC02). We acknowledge Emily Quinn, Dorathea Lee, and Andrew Campbell for assistance with SoLs purification.

Author contributions

E.A.O., J.Z., Y.-X.L., and J.L. designed research; E.A.O., J.Z., and Z.F. performed research. All authors analyzed data and discussed results. All authors participated in preparing the manuscript.

Competing Interests

The authors declare no competing interests.